VIII International Conference on Particle-Based Methods
PARTICLES 2023
U. Perego, M. Cremonesi, A. Franci (Eds)

DISCRETE ELEMENT METHOD APPROACH TO SIMULATE CREEP BEHAVIOR IN THERMAL BARRIER COATINGS

I. BENSEMMANE[1,2,3], W. LECLERC[1], N. FERGUEN[3], M. GUESSASMA[1] and M-E. DJEGHLAL[2]

[1] Laboratoire des Technologies Innovates (LTI)
Universit de Picardie Jules Verne
IUT de l'Aisne, 48 rue d'Ostende, 02100 Saint-Quentin, France

[2] Laboratoire Science et Gnie des Matriaux (LSGM)
Ecole Nationale Polytechnique
10 Rue des Frres Oudek, 16200 El Harrach, Algrie

[3] Centre de Dveloppement des Technologies Avances (CDTA)
Cit 20 aout 1956, 16303 Baba Hassen, Algrie

Abstract: Thermal Barrier Coatings (TBCs) are multilayer systems used in Ni-based superalloy components for gas turbine blades submitted to high temperatures resulting in the development of high thermal stresses. The intricacy of their microstructure coupled to severe environmental conditions lead to their premature failure according to complex mechanisms involving notably creep and Coefficient of Thermal Expansion (CTE) mismatch effects. This work aims to investigate the development of thermal residual stress within TBCs during a heating step using a numerical model based on Discrete Element Method (DEM). The suitability of such an approach is investigated in terms of stress field distribution in comparison to Finite Element Method (FEM). Results reveal the capability of the proposed DEM approach to simulate creep phenomenon in a TBC system under thermal loading and predict accurately thermal stresses leading to failure.

Keywords. Discrete Element Method, Thermal barrier coatings, Creep behavior, Norton's law, Thermal stresses

1 Introduction

TBCs are multilayered structures (Figure 1) applied on metallic parts operating at high temperature (T≈1100°C) and developed for numerous applications, including gas turbine engine, automotive heat management or aircraft propulsion. A TBC is typically composed of a ceramic top coat (TC), commonly an yttria stabilized zirconia (YSZ), an intermetallic Bond Coat (BC) and between them a Thermally Grown Oxide (TGO) that develops at high temperature. Such a system has demonstrated remarkable efficiency in optimizing the performance of turbine elements exposed to elevated temperatures [1], allowing a

surface temperature reduction of up to 300°C [2]. However, due to the complexity of their microstructure, a lack of reliable prediction of their life span and early stage of failure, the potential of TBCs cannot be fully employed. The failure in TBCs are related to several factors including the residual stress induced due to the coefficient of thermal expansion mismatch between layers of the TBC, the interface roughness of the TGO layer and the redistribution of stresses caused by creep effect at high temperature [3]. Most of numerical studies proposed to estimate stress distribution and failure mechanisms in TBCs are based on FEM. Thus, among other works, Ranjbar et al. [3] used an approach based on a 2D unit cell model of TBC with a sinusoidal profile to evaluate effects of the lamellar microstructure of TC on stress fields and failure mechanisms. Their study showed that crack evolution depends on oxide layer growth and interface roughness. Besides, Cen et al. [4] developed a similar approach to investigate stress distribution and failure during a thermal cycle, taking into account the growth of the TGO layer, thermal expansion and creep effect. As an alternative to FEM, the DEM was originally developed to solve different problems involving discrete particle systems [5] and later extended to simulate continuous elastic media. The main advantage of DEM is the possibility of handling with a large range of problems as complex crack propagation takes place [6–8]. It is worth noting that very few papers have reported on the simulation of thermal stresses and failure behavior of a TBC system using a DEM-based approach [9–11]. The studies carried out by Leclerc et al. [10] and Ferguen et al [11] put their emphasis on interfacial debonding and crack propagation considering a model based on real SEM images of TBC, taking into account the shape of the TGO layer, and temperature-dependent properties and CTE. In the present work, the 2D DEM framework originally introduced by Leclerc et al. [10] is extended and applied to investigate the creep effect on residual stresses during a heating step phase of the TBC. The paper is organized as follows: Section 2 provides a brief description of DEM-based approach used to simulate the thermomechanical behavior of TBC. Section 3 presents the validation of the proposed discrete element creep model based on Norton's law in the context of mechanical tensile tests. Section 4 is dedicated to an application of the developed DEM approach to simulate thermal stresses generated within a TBC system during a heating-up step due to combined effects of creep and thermal expansion. Finally, some remarks and conclusions are provided in section 5.

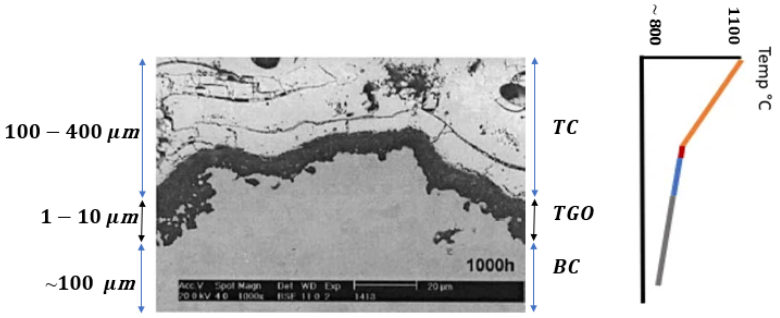

Figure 1: SEM cross-section of TBC system obtained by plasma spraying and related operating temperatures [12]

2 Thermomechanical modeling of a continuous medium by DEM

2.1 Hybrid lattice-particulate model

In the present work, the DEM is used to simulate the thermomechanical behavior of a TBC which can be considered as a multilayered continuous medium. The adopted approach, typically referred to as hybrid lattice particulate model [7,13] takes benefit of a randomly packed assembly of disks connected by cohesive Euler-Bernouli beam elements [13, 14] to represent a continuous material as depicted in Figure 2a and b. In our study, a 2D generation process is applied which allows for precise control of intrinsic properties of the random particulate system [13]. Typically, this is characterized by two main factors: i) the cardinal number which is defined as the average number of contacts per discrete element and is set to 4.6 and ii) the volume fraction of particles which is set to 85%. In addition, a slight polydispersity defined by a coefficient of variation of 0.3 is introduced to avoid directional effects and ensure system isotropy. The formulation of generalized cohesive force vector associated to each Euler-Bernoulli beam element introduced between each pair of particles in contact, depends on specific parameters such as beam length L_μ, cross-sectional area A_μ, quadratic moment I_μ, and the microscopic Young's modulus E_μ [15]. Acceleration, velocity and position of particles are defined according to Newton's second law of motion considering an explicit time-integration scheme. In the present work, we take benefit of velocity-Verlet scheme which allows us to accurately compute the positions and velocities of a large set of particles throughout the simulation.

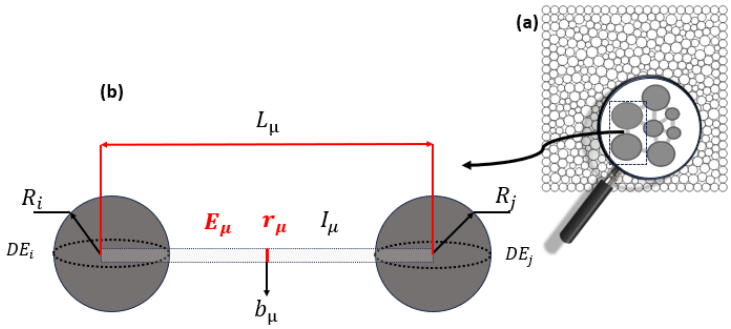

Figure 2: a) Particulate system. b) Zoom illustrating the cohesive beam model

2.2 Identification of macroscopic parameters of continuous medium

The relationship between the microscopic parameters E_μ and r_μ and the macroscopic Young's modulus E_M and Poisson's ratio ν_M is initially unknown. Consequently, the microscopic and macroscopic coefficients of the modeled continuum medium are commonly linked through calibration using polynomial functions P and Q as follows:

$$r_\mu = P(\nu_M) \tag{1}$$

$$E_\mu = Q(r_\mu)E_M \tag{2}$$

Haddad et al. [13] established calibration curves to relate E_μ and r_μ to macroscopic elastic properties of the material, E_M and ν_M. Subsequent work by Leclerc et al. [10] introduced a discrete model of TBC consisting of BC, TGO and TC layers in order to simulate failure mechanisms occuring during cooling step. In their work, each layer is assumed to be homogeneous and isotropic with temperature-dependent elastic properties. Based on calibration curves established by Haddad et al. [13], Leclerc et al. [10] identified specific microscopic parameters and their corresponding macroscopic elastic properties taken from the work of Cen et al. [4] for each layer of the TBC. Note that, in what follows, the discussed model lies on the numerical approach proposed by Leclerc et al. [10] and the same assumptions of mechanical behavior and elastic properties for each layer.

2.3 Thermal loading and expansion model

The main focus of this research is to simulate a gradual and linear heating phase of TBC, from 25°C to 1100°C up to the time duration of 300 seconds. Throughout the simulation, the particulate system is subjected to a uniform temperature. Besides, each layer of the TBC exhibits a distinctive response to the heating process due to its specific temperature-dependent CTE and creep parameters [4]. Thermal expansion effects are considered by adjusting the initial length of the cohesive beam elements $L_\mu(T_{init})$ with respect to the CTE of each layer and the applied temperature T [16] (see Figure 3) as follows:

$$L_\mu = L_\mu(T_{init})(1 + \alpha(T - T_{init})) \tag{3}$$

where α denotes the CTE of the corresponding layer.

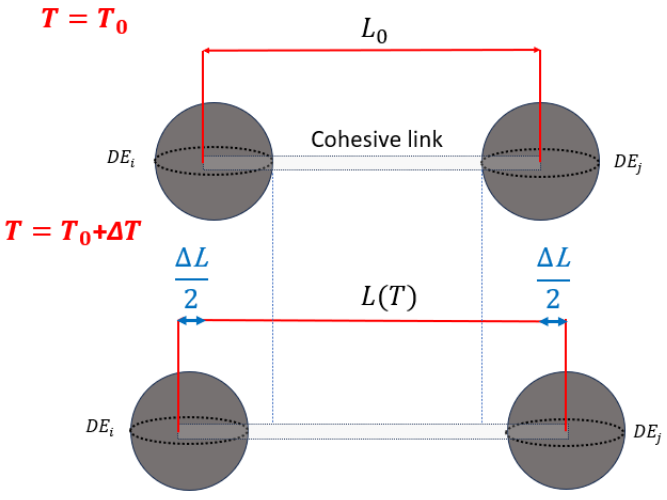

Figure 3: Thermal expansion model at the cohesive link scale

2.4 Stress field determination

In discrete simulations, Zhou's formulation is used to examine the stress field by linking the equivalent stress tensor to inter-particle contact forces and branch vectors between contacting particles as follows:

$$\overline{\overline{\sigma_i}} = \frac{1}{2\Omega_i} \sum_{j=1}^{Z_i} \frac{1}{2}(f_{ij} \otimes d_{ij} + f_{ij} \otimes d_{ij}) \tag{4}$$

where f_{ij} is the cohesion force vector applied to the particle i by a particle j, d_{ij} is the relative position vector between particles i and j and Z_i is the number of contacts between the particle i and its neighboring particles, Ω_i is the area of representation of the particle i. Although this formulation allows stress evaluation at the particle level, it is sensitive to local variations that could affect the overall results. To reduce this variation, the halo approach is introduced with the main aim of correcting stress estimation variability. This correction involves evaluating the stress tensor within a specific area at a mesoscopic scale guided by the formulation given in [17]. In our case, the halo is described by a circular geometry defined at the mesoscopic level for each Discrete Element (DE) which encompasses an adequate number of DEs (Figure 4), and thus allows stress determination for each DE, taking into account the contribution of the surrounding particles.

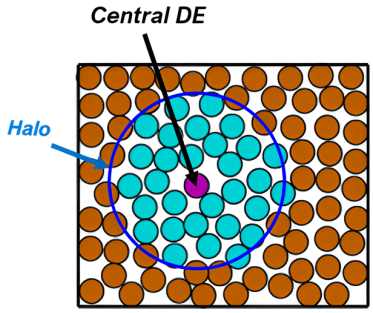

Figure 4: Definition of halo approach with surrounding particles (in blue) at the mesoscopic scale

3 DEM modeling of creep phenomena

3.1 Norton's model

Our current focus is to introduce a discrete creep model in the prospect to take into account such effects in the numerical simulation of a TBC upon heating step. The creep behavior describes how materials slowly deform under constant and high temperature. In the present work, Norton's law has been implemented in the model which enables to predict time-dependent deformation during the stationary creep (secondary stage) [18]. It considers both the time and the applied stress level to describe the creep deformation

over time according to the following equation:

$$\dot{\varepsilon} = B\sigma_{VM}^{n} \tag{5}$$

where $\dot{\varepsilon}$ is the strain rate, σ_{VM} is the Von-Mises stress, B is a constant depending on the material and n is the creep power law exponent (n=1 for visco-elastic materials, n>1 for visco-plastic ones). In our work, creep-induced strain is taken into account the same way as thermal expansion by adjusting cohesive element lengths so that two deformation contributions are associated to each beam element (creep and thermal expansion strain). By applying Zhou's approach discussed in subsection 2.4, the Von-Mises stress is calculated, considering a halo size of 5 for stress tensor computations, where the creep strain increment $\Delta\varepsilon$ for a time step Δt is given by:

$$\Delta\varepsilon = B\sigma_{VM}^{n}\Delta t \tag{6}$$

3.2 Validation test

As the first step of this work, creep tests are carried out on loaded samples in tension at constant load and temperature in order to validate the creep model implementation. For that purpose, we consider a 2D configuration as shown in Figure 5, for which a 2D rectangular system composed 44 100 DE is generated which satisfies criteria listed in subsection 2.1. The model has a length L=36μm and a width b=12μm and is submitted to a tensile force (F=10^{-6}N) on the right edge. Symmetry boundary conditions are imposed on the bottom and left edge so that the stress field is theoretically homogeneous. The tensile test is applied at high temperature (T=1100°C) on a homogeneous material for a duration of 2 hours for the TC material and 30 minutes for the BC ones.

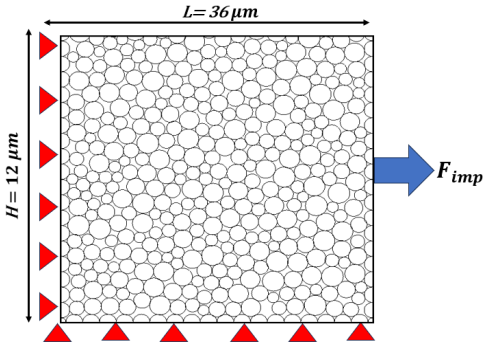

Figure 5: Tensile test configuration and applied boundary conditions

For validation purposes, creep displacement is compared with theoretical and FEM creep estimates as depicted in the results shown in Figure 6a and b. The graphics are presented for two cases involving visco-elastic TC and BC materials respectively and n and B parameters used in Norton's Law are listed in table 1 [4].

Table 1: Temperature-dependent data for creep parameters B and n used for TC, BC and TGO layers [4]

	Temperature [°C]	B [s^{-1}MPa^{-n}]	n
TC	750	1.8×10^{-11}	1
	1100	1.8×10^{-8}	1
TGO	750	7.3×10^{-12}	1
	1100	7.3×10^{-8}	1
BC	$\leq$ 600	6.54×10^{-19}	1
	700	2.2×10^{-12}	1
	800	1.84×10^{-7}	1
	$\geq$850	2.15×10^{-8}	1

DEM and FEM creep displacements over time were obtained by subtracting elastic displacement due the tensile force from the total one. The plotted curves are nearly confounded which confirms the validity of the proposed discrete creep model.

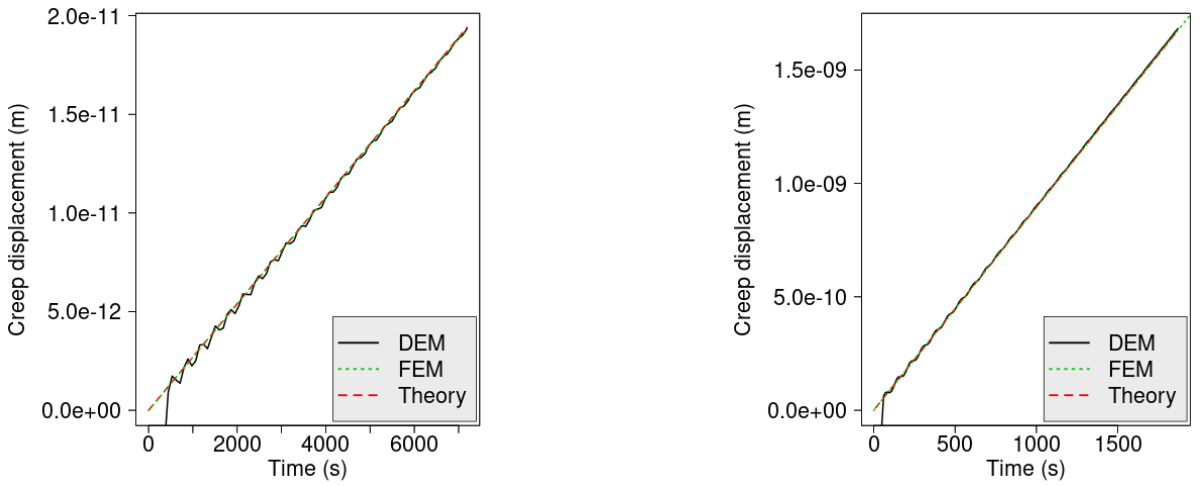

(a) Creep displacement for TC material

(b) Creep displacement for BC material

Figure 6: Creep displacement over the time for TC and BC materials

4 Application to the case of a TBC system subjected to a heating-up phase

4.1 Unit cell model of TBC

Figure 7 shows the employed unit cell model of TBC composed of 22 050 DE, which takes into account BC, TC and TGO layers and the interface roughness using a sinusoidal profile, the wavelength and amplitude of which are set at 12 and 5 micrometers, respectively [4, 19]. Symmetry boundary conditions are imposed on the bottom and right

sides of the model to represent only one half of the roughness. Note that, in the present study, DEM calculations are carried out using a halo size of 5.

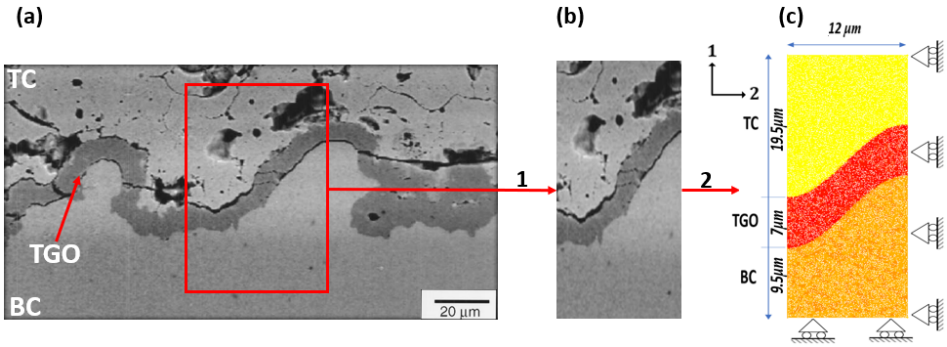

Figure 7: TBC unit cell model. a) SEM image of a TBC microstructure [20]. b) Extracted sample of interface roughness. c) DEM unit cell of TBC with configuration and applied boundary conditions

4.2 Von-Mises stress fields

4.2.1 Without creep effect

In a first step, FEM and DEM simulations have been conducted without creep effet in order to highlight the CTE mismatch between layers during heating at a high temperature resulting in thermal stresses. FEM and DEM stress predictions are shown in Figures 8a and b, respectively. σ_{VM} stress field is evaluated at the end of the heating step and only the CTE mismatch-induced strain is considered for each beam element. According to the DEM calculations, maximum stress value σ_{VM-max} is located at the peak region within the TGO layer near the BC/TGO interface and this observation is in good agreement with that given by FEM one. σ_{VM} stress values are higher near the BC/TGO interface since the CTE mismatch is more important between BC and TGO layers. DEM stress calculations show that the maximum value σ_{VM-max} is equal to 1490 MPa vs. 1446 MPa for FEM. In addition, the minimum value σ_{VM-min} is located within the TC layer due to low CTE mismatch between TC and TGO layers [4], as also observed in FEM calculations.

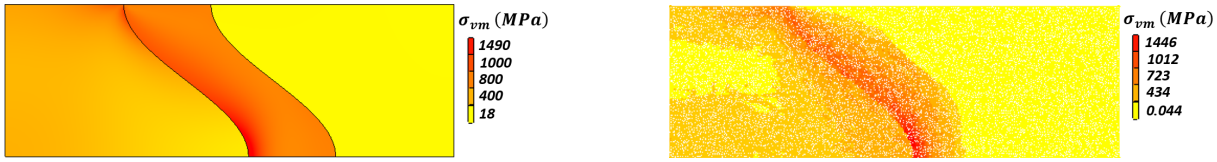

(a) σ_{VM} stress distribution obtained by FEM

(b) σ_{VM} stress distribution obtained by DEM

Figure 8: Von-Mises stress field distribution without creep at the end of the heating-up phase

4.2.2 With creep effect

We now consider the creep contribution in order to investigate its effect on the Von-Mises stress field distribution. We can observe on Figures 9a and b relative to FEM and DEM simulations that the locations of maximal Von-Mises σ_{VM-max} and minimal Von-Mises σ_{VM-min} stress values are close to that observed without creep. Besides, a quite good agreement is again observed between FEM and DEM with σ_{VM-max} respectively equal to 605 MPa and 566 MPa. Compared to the configuration without creep, Von-Mises stresses fields are reduced for both FEM and DEM due to their redistribution along the TGO layer near the BC/TGO interface as shown in Figure 9a and b.

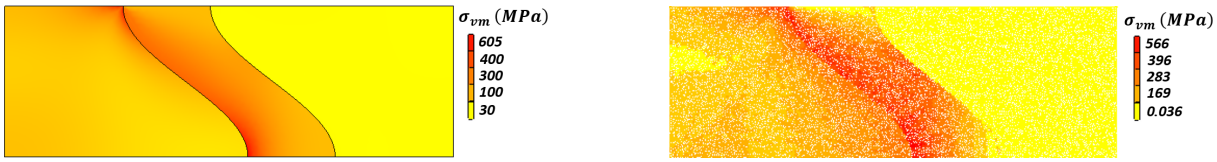

(a) σ_{VM} stress distribution obtained by FEM (b) σ_{VM} stress distribution obtained by DEM

Figure 9: Von-Mises stress field distribution with creep included at the end of the heating phase

Note that the stress reduction appears at about 700°C, as seen for the maximal Von-Mises stress evolution curve as function of applied temperature in Figure 10, when creep occurs for all layers of the TBC as listed in Table 1.

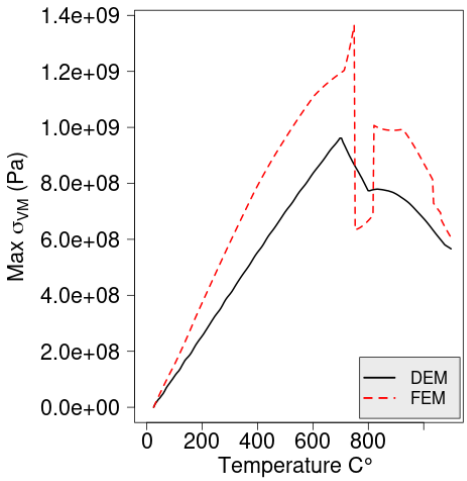

Figure 10: Maximal Von-Mises stress evolution as function of applied temperature

5 Conclusion

DEM-based approach was proposed to simulate the creep behavior of a TBC during a heating step. In first step, tensile validation tests were performed on a homogeneous

materials at high temperature (T=1100°C), the comparison between DEM, FEM and theoretical creep displacement exhibited a quite good agreement. In a second step, the DEM-based approach was applied to the case of a TBC with a sinusoidal interface profile with the three layers as visco-elastic materials. Von-Mises stress field was evaluated and compared to FEM simulations for two cases, with and without creep. For the two cases, σ_{VM-max} was located for both DEM and FEM at the peak region of the TGO layer near the BC/TGO interface with a slight difference of value. When adding creep, reduction of Von-Mises stress was observed, the results obtained from both DEM and FEM simulations displayed a good agreement.

In a next future, we expect to simulate a complete thermal cycle including dwelling and cooling-down steps and taking into account the visco-plasticity of the BC layer. We also project to numerically simulate failure mechanisms based on realistic SEM images.

REFERENCES

[1] R. Vassen, G. Kerkhoff and D. Stover. Development of a micromechanical life prediction model for plasma sprayed thermal barrier coatings. *Materials Science and Engineering: A*, 303(1-2):100–109, 2001.

[2] S-W. Myoung, S-S. Lee, H-S. Kim, M-K. Kim, Y-G. Jung and al. Effect of post heat treatment on thermal durability of thermal barrier coatings in thermal fatigue tests. *Surface and Coatings Technology*, 215:46–51, 2013.

[3] M. Ranjbar-Far, J. Absi, G. Mariaux and F. Dubois. Simulation of the effect of material properties and interface roughness on the stress distribution in thermal barrier coatings using finite element method. *Materials & Design*, 31(2):772–781, 2010.

[4] L. Cen, W-Y. Qin and Q-M. Yu. Analysis of interface delamination in thermal barrier coating system with axisymmetric structure based on corresponding normal and tangential stresses. *Surface and Coatings Technology*, 358:785–795, 2019.

[5] P-A. Cundall. Rational design of tunnel supports: A computer model for rock mass behavior using interactive graphics for the input and output of geometrical data. Technical report, Minnesota University Minneapolis Department of Civil and Mining Engineering, 1974.

[6] A. Ammar, W. Leclerc, M. Guessasma and N. Haddar. Discrete element approach to simulate debonding process in 3D short glass fibre composite materials : Application to PA6/GF30. *Composite Structures*, 270:114035, 2021.

[7] D. André, I. Iordanoff, J. Charles and J. Néauport. Discrete element method to simulate continuous material by using the cohesive beam model. *Computer methods in applied mechanics and engineering*, 213:113–125, 2012.

[8] N. Ferguen, Y. Mebdoua-Lahmar, H. Lahmar, W. Leclerc and M. Guessasma. Dem model for simulation of crack propagation in plasma-sprayed alumina coatings. *Surface and Coatings Technology*, 371:287–297, 2019.

[9] M-A. Ghasemi and S-R. Falahatgar. Discrete element simulation of damage evolution in coatings. *Granular Matter*, 22(2):1–16, 2020.

[10] W. Leclerc, N. Ferguen and E-S. Lamini. Discrete element method to simulate interface delamination and fracture of plasma-sprayed thermal barrier coatings. *Modelling and Simulation in Materials Science and Engineering*, 30(4):045012, 2022.

[11] N. Ferguen, W. Leclerc and E-S. Lamini. Numerical investigation of thermal stresses induced interface delamination in plasma-sprayed thermal barrier coatings. *Surface and Coatings Technology*, page 129449, 2023.

[12] H-D. Echslerand Renusch and M. Schütze. Bond coat oxidation and its significance for life expectancy of thermal barrier coating systems. *Materials Science and Technology*, 20(3):307–318, 2004.

[13] H. Haddad, W. Leclerc, M. Guessasma, C. Pélegris, N. Ferguen and E. Bellenger. Application of DEM to predict the elastic behavior of particulate composite materials. *Granular Matter*, 17(4):459–473, 2015.

[14] W. Leclerc. Discrete element method to simulate the elastic behavior of 3D heterogeneous continuous media. *International Journal of Solids and Structures*, 121:86–102, 2017.

[15] W. Leclerc, H. Haddad and M. Guessasma. On the suitability of a Discrete Element Method to simulate cracks initiation and propagation in heterogeneous media. *International Journal of Solids and Structures*, 108:98–114, 2017.

[16] G. Alhajj Hassan, W. Leclerc, C. Pélegris, M. Guessasma and E. Bellenger. On the suitability of a 3D discrete element method to model the composite damage induced by thermal expansion mismatch. *Computational Particle Mechanics*, 7(4):679–698, 2020.

[17] D. Moukadiri, W. Leclerc, K. Khellil, Z. Aboura, M. Guessasma and al. Halo approach to evaluate the stress distribution in 3d discrete element method simulation: Validation and application to flax/bio based epoxy composite. *Modelling and Simulation in Materials Science and Engineering*, 27(6):065005, 2019.

[18] T-H. Hyde, W. Sun and C-J. Hyde. *Applied creep mechanics*. 2014.

[19] M. Bäker. Finite element simulation of interface cracks in thermal barrier coatings. *Computational Materials Science*, 64:79–83, 2012.

[20] E-A. Rabiei and A-G. Evans. Failure mechanisms associated with the thermally grown oxide in plasma-sprayed thermal barrier coatings. *Acta materialia*, 48(15):3963–3976, 2000.